C. R. Physique 15 (2014) 587–598

Contents lists available at ScienceDirect

Comptes Rendus Physique

www.sciencedirect.com

Emergent phenomena in actinides / Phénomènes émergents dans les actinides

# Multipole fluctuations of itinerant f electrons and triakontadipole order in $URu_2Si_2$

## *Fluctuations des multipoles dans les systèmes à électrons f itinérants et ordre triacontadipolaire dans $URu_2Si_2$*

Hiroaki Ikeda [a,b,*], Michi-To Suzuki [c,d], Ryotaro Arita [c], Tetsuya Takimoto [e]

[a] *Department of Physics, Ritsumeikan University, Kusatsu 525-8577, Japan*
[b] *Department of Physics, Kyoto University, Kyoto 606-8502, Japan*
[c] *RIKEN Center for Emergent Matter Science (CEMS), Wako, Saitama 351-0198, Japan*
[d] *CCSE, Japan Atomic Energy Agency, 5-1-5 Kashiwanoha, Kashiwa, Chiba 277-8587, Japan*
[e] *Department of Physics, Hanyang University, Seongdong, Seoul 133-791, Republic of Korea*

ARTICLE INFO

*Article history:*
Available online 26 July 2014

*Keywords:*
Hidden order
$URu_2Si_2$
Multipolar order
Multipolar fluctuations

*Mots-clés :*
Ordre caché
$URu_2Si_2$
Ordre multipolaire
Fluctuations de multipôle

ABSTRACT

Novel electronic states are hallmarks of strongly correlated f-electron systems. The spin–orbital coupled degrees of freedom can lead to an exotic type of multipole hidden order (HO). A well-known HO is observed at the 17.5 K phase transition in $URu_2Si_2$, which is a long-standing mystery since its discovery in 1985. The dominating itinerant character of the 5f electrons complicates a theoretical description of this phenomenon. Here we review recent progress on a first-principles theoretical approach that allows catching the itinerant feature of f electrons. We show that in the itinerant 5f-electron model of $URu_2Si_2$, the most divergent multipole susceptibility indicates an instability to a triakontadipole order, with a doubly degenerate *E*-type symmetry. This itinerant-type multipole order is consistent with key features in the HO state, including the broken fourfold rotational symmetry observed in recent experiments.

© 2014 Académie des sciences. Published by Elsevier Masson SAS. All rights reserved.

RÉSUMÉ

Les systèmes à électrons f fortement corrélés sont souvent caractérisés par des états électroniques nouveaux. Les degrés de liberté couplés par l'interaction spin–orbite peuvent donner lieu à un ordre exotique, *caché*, des moments multipolaires. Un exemple bien connu d'ordre caché est celui qui se développe à la transition de phase observée à 17,5 K dans $URu_2Si_2$, qui constitue un mystère depuis sa découverte en 1985. Le caractère itinérant des électrons 5f dans $URu_2Si_2$ complique la description théorique de ce phénomène. Nous passons en revue les progrès récents accomplis sur la base d'un traitement théorique *ab initio* qui permet de décrire ce caractère itinérant. Nous montrons que, dans ce modèle, les divergences des susceptibilités multipolaires indiquent une instabilité vers un ordre triacontadipolaire, avec une symétrie de type E. Cet ordre multipolaire de type itinérant

* Corresponding author at: Department of Physics, Ritsumeikan University, Kusatsu 525-8577, Japan.
*E-mail address:* ikedah@fc.ritsumei.ac.jp (H. Ikeda).

http://dx.doi.org/10.1016/j.crhy.2014.07.002
1631-0705/© 2014 Académie des sciences. Published by Elsevier Masson SAS. All rights reserved.

est compatible avec les principales caractéristiques de l'état d'ordre caché dans $URu_2Si_2$, y compris une rupture de la symétrie de rotation d'ordre 4 telle qu'observée dans le cadre d'expériences récentes.

© 2014 Académie des sciences. Published by Elsevier Masson SAS. All rights reserved.

## 1. Introduction

The intermetallic compounds containing elements with 4f or 5f electrons are called heavy-fermion materials due to the presence of electrons with a large effective mass, up to 1000 times the free-electron mass. In these f-electron systems, strong electron correlations and high degeneracy of the f-electron multiplets can lead to novel electronic states, such as complex magnetic/multipole order, quantum critical electronic matter, unconventional superconductivity, and so on. When we investigate microscopically the origin of these phenomena, we are faced with the fact that the electronic band structure in these materials is very complicated, and also that the electron correlation is very strong. The complicated band structure is a serious problem, especially if an itinerant character of the f electrons is dominating in the intermediate correlation regime. This is a bottleneck to understand the essence of various attractive phenomena in heavy-fermion materials from the microscopic viewpoint. On the other hand, the complicated electronic structure is closely related to various kinds of novel electronic states. Thus, it is indispensable to derive useful information from first-principles calculations of the electronic structure. For this purpose, the development of suitable first-principles calculation approaches has been a central issue of condensed-matter physics for the last decades.

Recently, in the first-principles calculations based on density-functional theory (DFT), the efficiency of several methods for treating electron correlations has been settled. For instance, the DFT + $U$ method can describe the strong correlation limit of f electrons, whereas the DFT + DMFT (dynamical mean-field theory) method [1,2] successfully interpolates between weak and strong correlations. Moreover, a downfolding approach based on Wannier functions [3] makes it possible to construct an effective multi-orbital model and analyze it with several efficient numerical calculations. Such progress on the first-principles theoretical approach shed light on long-standing mysteries in heavy-fermion materials. The hidden order in $URu_2Si_2$ that we introduce in this review is one of the most difficult problems among them. Although this order is characterized by a clear jump of the specific heat at $T_{HO} = 17.5$ K [4,5], its nature remains enigmatic three decades after its discovery in 1985. In this article, we review the current stage of the first-principles theoretical approach for this problem [6,7]. We show that the most divergent susceptibility in an itinerant f-electron model, which is constructed by the Wannier technique from first-principles calculations, indicates an instability into a kind of multipole (triacontadipole) density wave. This itinerant multipole order naturally provides comprehensive explanations of all key features in the hidden-order (HO) phase, including anisotropic magnetic excitations, nearly degenerate antiferromagnetic (AFM) ordered state, and spontaneous rotational symmetry breaking. Therefore it is a promising candidate for the HO parameter of $URu_2Si_2$.

In the following section, we provide a brief introduction on several physical properties of $URu_2Si_2$ and on the present status of first-principles modelling. Then, we describe our methodology in the Wannier-based approach and the obtained multipole correlation functions in the antiferroic triacontadipole density-wave state. Finally, we summarize the current status of our understanding of $URu_2Si_2$.

### 1.1. Brief introduction to $URu_2Si_2$

In 1985, it was found that $URu_2Si_2$, a compound crystallizing in the $ThCr_2Si_2$-type body-centered tetragonal structure ($I4/mmm$), shows two phase transitions, at $T_{HO} = 17.5$ K and $T_C = 1.4$ K [4,5], as shown in Fig. 1a. The enhanced specific-heat Sommerfeld coefficient indicates that this material is an heavy fermion. It was immediately confirmed that the low-temperature phase transition at $T_C = 1.4$ K corresponds to the emergence of unconventional superconductivity, which is also interesting due to a possible chiral $d$-wave state [8]. On the other hand, although the phase transition at $T_{HO} = 17.5$ K shows a textbook example of the specific heat jump expected for a second-order transition in a mean-field approximation, the precise nature of the associated order parameter remains unclear [6].

In the early stage, the observation by neutron scattering techniques of AFM order with a tiny moment ($\sim 0.03\mu_B$) attracted considerable attention [9]. However, later experiments suggested that the origin of the tiny moment could be related to inhomogeneity or disorder at ambient pressure. On the other hand, an AFM state with a larger ordered moment is stabilized upon compression [10,11]. Interestingly, in the pressure–temperature ($P$–$T$) phase diagram (Fig. 1b), the transition temperature changes gradually with applying pressure, but the transition from the HO to the AFM state is first-order-like. In addition, the Fermi surfaces in both ordered states are strikingly similar [12,13]. This indicates that a Fermi-surface reconstruction due to antiferroic folding occurs also in the HO state, as partially confirmed by angle-resolved photoemission spectroscopy (ARPES) [14–16]. Such Fermi-surface gapping is consistent with the formation of a gap observed by scanning tunneling microscopy [17,18] and with the dramatic decrease of carriers revealed below $T_{HO}$ by Hall effect measurements

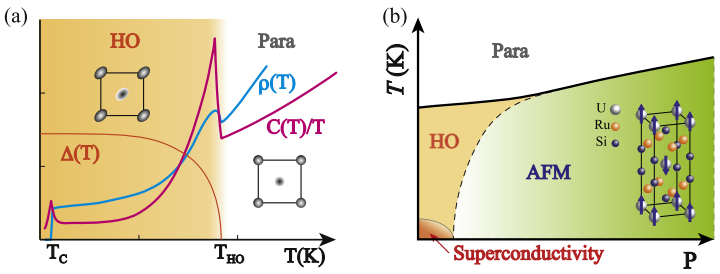


**Fig. 1.** (Color online.) (a) Phase transitions in $URu_2Si_2$, observed in resistivity $\rho(T)$ and specific heat $C(T)/T$. A schematic view of the in-plane fourfold rotational symmetry breaking is shown in the insets. $\Delta(T)$ denotes the HO parameter. (b) Schematic $P$–$T$ phase diagram. The inset shows the crystal structure and the spin configuration in the AFM state.

[8,19]. Closely related to these charge-gap formation, neutron inelastic scattering [9,20,21] indicates a gap formation in the magnetic excitation spectra at commensurate $Q_0 = (0\ 0\ 1)$ and incommensurate $Q_1 = (0.6\ 0\ 0)$ reciprocal space positions. Furthermore, a breaking of the in-plane fourfold rotational symmetry has been advocated by magnetic torque measurements [22], cyclotron resonance experiments [23], and high-resolution X-ray diffraction measurements [24,25]. In addition, a cusp-like structure observed in the NMR Knight shift under in-plane field rotation provides microscopic evidence for rotational symmetry breaking [26]. These new aspects restrict possible candidates for the HO parameter, which must be compatible with a doubly degenerate $E$-type state [27]. So far, whenever new experimental results have been reported, new theoretical models have been proposed [28–45]. Nevertheless, the nature of the HO transition remains unclear. In order to elucidate its essence, a quantitative understanding is compulsory. In this regard, recent progress on the first-principles approach gives us a chance to uncover the enigmatic HO transition completely.

### *1.2. Attempts based on first-principles calculations*

Here, we briefly review several studies based on first-principles calculations. First of all, S. Elgazzar et al. [35] calculated the large-moment AFM state based on the LSDA. From the similarity of the Fermi surface in both HO and AFM states, they considered a dynamical AFM order. Although they did not clarify any genuine order parameter, it was suggested that a folding of the Fermi surface by antiferroic order with a $Q_0 = (1\ 0\ 0)$ propagation vector is important, even in the HO phase. Furthermore, from the fact that the Fermi surface in a localized f-electron case is incompatible with experimental results, Oppeneer et al. [46] have concluded that the f electrons in this material should be itinerant rather than localized. Next, based on the LSDA + $U$ method, Cricchio et al. [36] found that although the ordered magnetic dipole moment can be small, a rank-5 multipole moment develops at the large $U$ limit. Thus they suggested that the HO state is a rank-5 triacontadipole order, with the same irreducible representation (IR) $A_2^-$ of the AFM order along the $c$-axis. Based on the DFT+DMFT method, Haule and Kotliar [37] calculated the one-particle excitation spectra, and analyzed the crystalline electric field (CEF) assuming almost localized f electrons. Based on the obtained CEF scheme, they suggested an antiferroic $A_2^+$ hexdecapole order. This proposed order parameter, however, is inconsistent with recent reports of a fourfold symmetry breaking [22–26]. In addition, it is not clear what would be the ground state over a wide range of the interaction parameters. This is an interesting subject for future work.

## 2. New trend on the first-principles approach

Generally speaking, a second-order transition is signaled by a divergence of a relevant susceptibility. Therefore, we can find possible phase transitions by investigating the $Q$ structure of the susceptibilities in the paramagnetic state. Indeed, for d-electron systems, studying susceptibilities within random-phase approximation (RPA) is current practice. On the other hand, for f-electron heavy-fermion systems, since the electronic band structure is much more complicated, this important step of the study is not common. However, recent Wannier-based down-folding [47] based on first-principles calculations provide us with low-energy effective models, i.e. multi-orbital tight-binding models, allowing us to take into account proper material-dependent information theoretically. Indeed, such theoretical approach has been already applied to several multi-orbital systems, such as the iron-pnictide superconductors [48]. In this review, we introduce the first application [7] to itinerant f-electron systems with the spin–orbit coupling.

### *2.1. Construction of the effective model*

First of all, relativistic electronic structure calculations are carried out by using the GGA–PBE exchange-correlation functional and the augmented plane wave plus atomic orbitals method, as implemented in the WIEN2K package [49]. The crystallographic parameters are taken from experiments [50]. The obtained band structure (Fig. 2a) is consistent with previous studies [12,46]. Next, the down-folded tight-binding Hamiltonian is constructed using the WANNIER90 code [51] via WIEN2WANNIER interface [47]. The localized Wannier functions are composed of U(5f), U(6d), Ru(4d) and Si(3p) states.

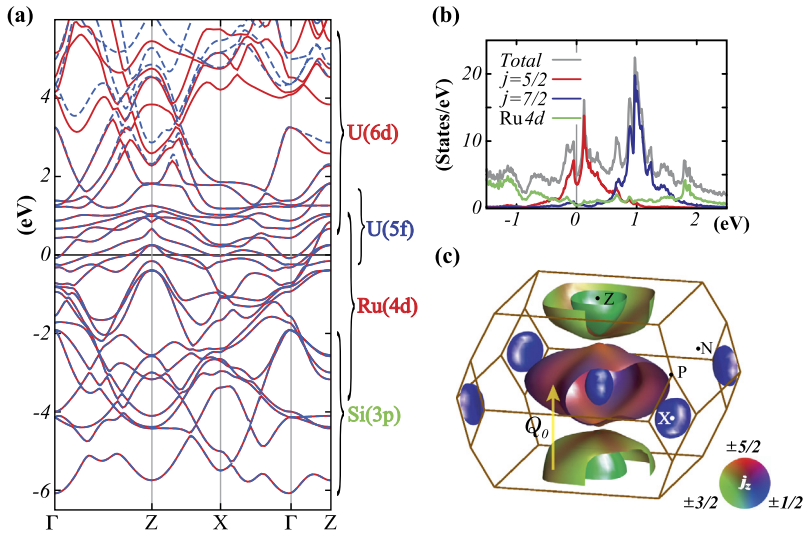


**Fig. 2.** (Color online.) (a) Electronic band structure obtained by first-principles calculations (red lines) and its Wannier fit (blue dashed lines). (b) Partial DOS. (c) $j$-Resolved Fermi surface in the paramagnetic state. Two outer Fermi surfaces are well nested with $Q_0 = (0\ 0\ 1)$.

The obtained tight-binding model reproduces well the first-principles band structure. This real-space representation model Hamiltonian facilitates the extraction of orbital-resolved information. For instance, orbital-resolved Fermi surfaces, as shown below, reveal details that cannot be recognized by an examination of the total Fermi surface. The construction of the effective model has been completed by adding the Hubbard-type interaction,

$$H' = \frac{U}{2}\sum_{i\ell}\sum_{\sigma} f^{\dagger}_{i\ell\sigma} f^{\dagger}_{i\ell\bar{\sigma}} f_{i\ell\bar{\sigma}} f_{i\ell\sigma} + \frac{U'}{2}\sum_{i\ell\neq m}\sum_{\sigma\sigma'} f^{\dagger}_{i\ell\sigma} f^{\dagger}_{im\sigma'} f_{im\sigma'} f_{i\ell\sigma} + \frac{J}{2}\sum_{i\ell\neq m}\sum_{\sigma\sigma'} f^{\dagger}_{i\ell\sigma} f^{\dagger}_{im\sigma'} f_{i\ell\sigma'} f_{im\sigma} + \frac{J'}{2}\sum_{i\ell\neq m}\sum_{\sigma} f^{\dagger}_{i\ell\sigma} f^{\dagger}_{i\ell\bar{\sigma}} f_{im\bar{\sigma}} f_{im\sigma} \tag{1}$$

The obtained Anderson lattice model is a 56-orbital model [7]. Hereafter, we measure the interaction parameters in units of $1/\rho_f$, where $\rho_f = 4.20$(states/eV) is the f-electron density of states at the Fermi level.

### 2.2. Density of states, Fermi surface, and mass renormalization

Fig. 2b shows partial density of states (DOS),

$$\rho_{\ell}(\omega) = \sum_{nk} \left|u^{k}_{\ell n}\right|^2 \delta(\omega - \epsilon_{nk}) \tag{2}$$

where $\epsilon_{nk}$ and $u^{k}_{\ell n}$ denote respectively the $n$th energy eigenvalue and its unitary matrix element with orbital label $\ell$. Electronic states near the Fermi level are dominated by the total angular momentum multiplet $j = 5/2$ of U(5f). Two f electrons occupy this state. On the other hand, the majority of the $j = 7/2$ multiplet is located at $\sim$1 eV higher. Its occupation number is 0.7. However, the inclusion of on-site interactions suppress this value. In practice, we can consider the $j = 7/2$ multiplet as unoccupied and we neglect hereafter its contribution.

Fig. 2c depicts the Fermi surface colored by the weight of the $j_z$ component. One can see that each separated Fermi surface is dominated by a specific $j_z$ component, except for the outer Fermi surface around the $Z$ point. This orbital-resolved Fermi surface is quite helpful in that we can capture valuable information about orbital characters on the Fermi-surface nesting, which play an essential role for the HO transition. The outer electron Fermi surface around the $\Gamma$ point is well nested with the outer hole Fermi surface around the $Z$ point with $Q_0 = (0\ 0\ 1)$.

Before proceeding to the discussion of susceptibilities, we stress that our approach is based on the Fermi-liquid theory. In heavy-fermion systems, the effective mass of quasi-particles is strongly enhanced due to renormalization effects. Experimental results, such as the specific heat, give in this case a mass enhancement of around 10. Hereafter, by considering this effect, the energy scale of the tight-binding hopping integrals is reduced by a factor of 10. This does not affect the $Q$ structure of susceptibilities, but makes comparisons with the experiments straightforward. This assumption holds only when the renormalized quasi-particles Fermi surface is not very different from the original Fermi surface. Recently reported ARPES data [52] have indicated that the f-electron bands are dispersive, and an itinerant f-electron model based on first-principles calculations is a good starting point.

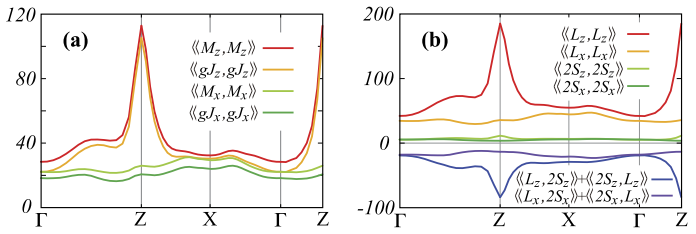


**Fig. 3.** (Color online.) (a) Magnetic correlations, $\langle\langle M_\mu, M_\mu\rangle\rangle$ and $\langle\langle gJ_\mu, gJ_\mu\rangle\rangle$, along high-symmetry lines, where $M_\mu = L_\mu + 2S_\mu$ with $\mu = (x, y, z)$. (b) Orbital and spin contributions. The orbital contribution (red) is much larger than the spin contribution (green). The correlation between orbital and spin (blue) is negative.

## 3. Two-body correlation functions

### 3.1. Magnetic susceptibilities

The generalized susceptibility in multi-orbital systems is evaluated as

$$\chi^0_{\ell m,\ell' m'}(q) = -T\sum_{k,n} G^0_{\ell\ell'}(k+q, \mathrm{i}\omega_n) G^0_{m'm}(k, \mathrm{i}\omega_n) \tag{3}$$

where $\omega_n$ are Matsubara frequencies, and $G^0_{\ell\ell'}(k, \mathrm{i}\omega_n)$ is the bare Green's function,

$$G^0_{\ell\ell'}(k, \mathrm{i}\omega_m) = \sum_n \frac{u^k_{\ell n} u^{k\,*}_{\ell' n}}{\mathrm{i}\omega_m - \varepsilon_{nk} + \mu} \tag{4}$$

For instance, in operators of total angular momentum,

$$\hat{J}_{z(x)} = \sum_{m=\pm 5/2, \pm 3/2, \pm 1/2} (J_{z(x)})_{\ell m} f^\dagger_{i\ell} f_{im} \tag{5}$$

$J_z$ and $J_x$ are given by

$$J_z = \begin{pmatrix} \frac{5}{2} & & & & & \\ & \frac{3}{2} & & & & \\ & & \frac{1}{2} & & & \\ & & & -\frac{1}{2} & & \\ & & & & -\frac{3}{2} & \\ & & & & & -\frac{5}{2} \end{pmatrix}, \qquad J_x = \begin{pmatrix} 0 & \frac{\sqrt{5}}{2} & & & & \\ \frac{\sqrt{5}}{2} & 0 & \sqrt{2} & & & \\ & \sqrt{2} & 0 & \frac{3}{2} & & \\ & & \frac{3}{2} & 0 & \sqrt{2} & \\ & & & \sqrt{2} & 0 & \frac{\sqrt{5}}{2} \\ & & & & \frac{\sqrt{5}}{2} & 0 \end{pmatrix} \tag{6}$$

in the matrix form in the $j = 5/2$ subspace, $j_z = (5/2, 3/2, 1/2, -1/2, -3/2, -5/2)$. In this case, as $A(B) = J_{z(x)}$, the magnetic susceptibility between $A$ and $B$ is defined as:

$$\langle\langle A, B\rangle\rangle = \sum_{\ell\ell' mm'} A_{m\ell} \chi_{\ell m,\ell' m'}(q) B_{\ell' m'} \tag{7}$$

where $\chi_{\ell m,\ell' m'}(q)$ is $\chi^0_{\ell m,\ell' m'}(q)$ in the unperturbed case, and in the RPA

$$\hat{\chi}^{\mathrm{RPA}}(q) = \hat{\chi}^0(q) + \hat{\chi}^0(q)\hat{\Gamma}^0\hat{\chi}^{\mathrm{RPA}}(q) \tag{8}$$

where $\hat{\Gamma}^0$ is the Hubbard-type interaction in the matrix form. In Fig. 3a, we show magnetic susceptibilities for $U = U' \simeq 2.3$ and $J = J' = 0$. A remarkable peak at $Z$ (0 0 1) in the $J_z$–$J_z$ correlation corresponds to the Fermi-surface nesting, while the in-plane $J_x$–$J_x$ ($J_y$–$J_y$) correlation is inactive. It is very interesting that remarkable magnetic anisotropy appears in an itinerant model. This anisotropy comes from different orbital components on the nested Fermi surface between the outer sheets around $\Gamma$ and $Z$ points. These Fermi surfaces are mainly constructed from $\pm 5/2$ and $\mp 3/2$ components, as shown in Fig. 4. To connect these components, the angular momentum change of $4\hbar$ is a prerequisite. However, the angular momentum change accompanied by $J_{x(y)}$ is only $1\hbar$. Therefore, the in-plane susceptibility is not enhanced.

In Fig. 3b, magnetic susceptibilities are divided into several susceptibilities between spin and orbital moments. The orbital correlation is much larger than the spin correlation, and the correlation between spin and orbital moments is negative. This just corresponds to U(5f) being less than onehalf. Moreover, the magnetic $M_z$ correlation is almost the same as the $gJ_z$ correlation with Landé $g$-factor $g = 6/7$. This means that the Van Vleck susceptibility into the $j = 7/2$ multiplet provides only a small shift, independent of $Q$. For this reason, neglecting $j = 7/2$ contributions is an acceptable approximation.

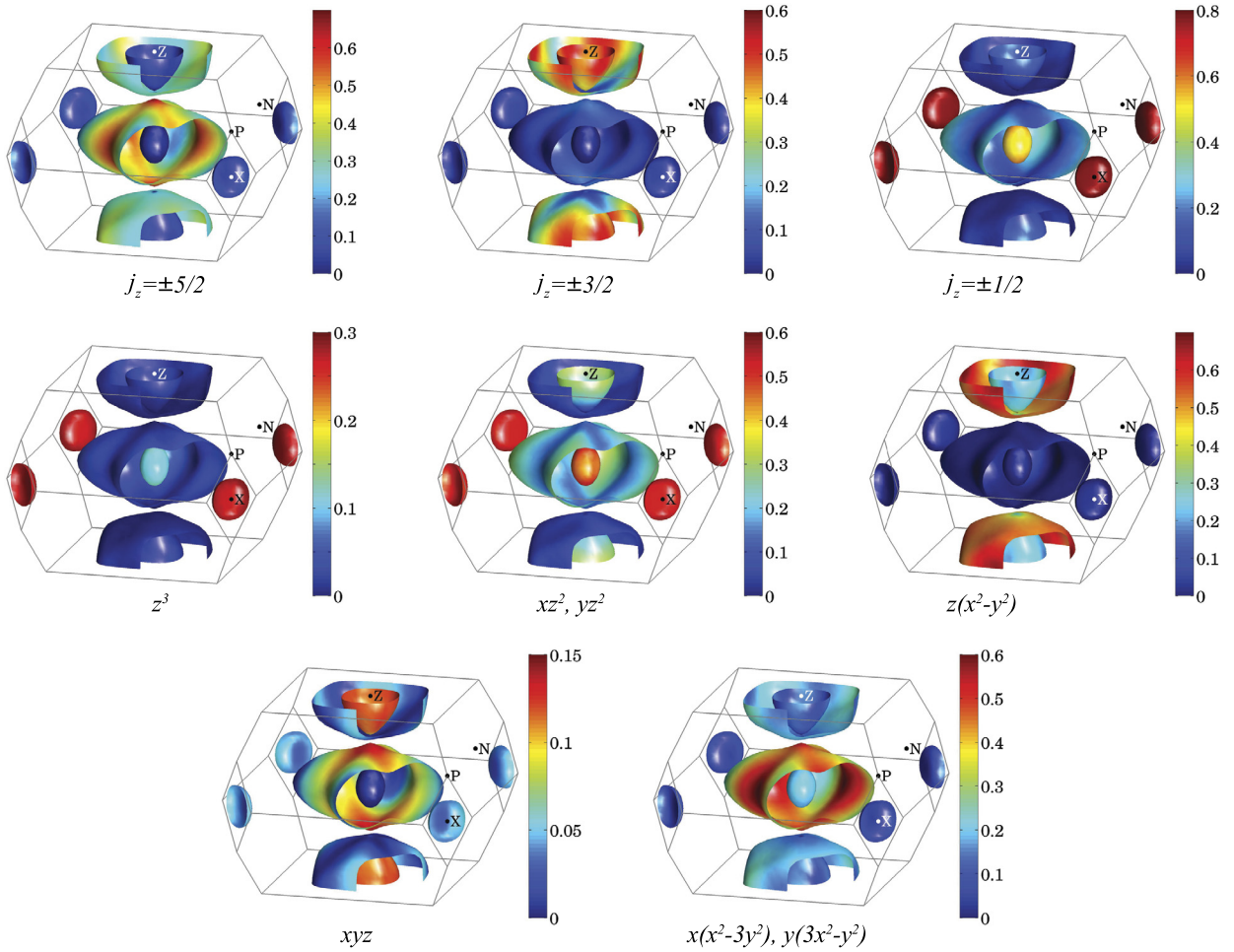


**Fig. 4.** (Color online.) Fermi surfaces colored by orbital contributions.

Another characteristic feature is a hump structure at the incommensurate $Q_1 = (0.6\ 0\ 0)$ reciprocal space position. This $Q_1$ vector corresponds to the one at which an inelastic peak is observed in neutron scattering spectra [9,20,21]. Thus, it is expected that two specific $Q$ vectors are closely related to the Fermi surface topology.

### 3.2. Multipole moments

In multi-orbital systems, orbital fluctuations (such as quadrupole ones) can give rise to an angular momentum change of $2\hbar$. In other words, this is rank 2. In the $j = 5/2$ multiplet, the highest rank is 5, which corresponds to a transition between $\pm 5/2$ and $\mp 5/2$. The $j = 5/2$ subspace contains six orbitals from $j_z = +5/2$ to $-5/2$. The degrees of freedom of the particle-hole pair $f^{\dagger}_{i\ell} f_{im}$ are $6 \times 6 = 36$.

Table 1 represents the group-theoretical classification under tetragonal symmetry of these 36 multipole moments, except for rank 0. Here, rank 1 denotes dipole, rank 2 quadrupole, rank 3 octupole, rank 4 hexadecapole, rank 5 triacontadipole. These representation matrices can be straightforwardly calculated from the operator-equivalent method. For instance, rank-5 $D_4$ and $D_x$ are given by

$$D_4 = \begin{pmatrix} & & & & -0.50\mathrm{i} & \\ & & & 0.00\mathrm{i} & & 0.50\mathrm{i} \\ & & 0.00\mathrm{i} & & 0.00\mathrm{i} & \\ & 0.00\mathrm{i} & & 0.0\mathrm{i}0 & & \\ 0.50\mathrm{i} & & 0.00\mathrm{i} & & & \\ & -0.50\mathrm{i} & & & & \end{pmatrix}$$

**Table 1**
Classification of multipoles except for rank 0 under tetragonal symmetry. ± denotes the parity for time reversal. $D_{x(y)}$ is defined by $D_{x(y)} \equiv (D_{x(y)a1} + D_{x(y)a2} + D_{x(y)b})/\sqrt{3}$.

| Rank | $A_1^+$ | $A_2^+$ | $B_1^+$ | $B_2^+$ | $E^+$ |
|---|---|---|---|---|---|
| 2 | $O_{20}$ | | $O_{22}$ | $O_{xy}$ | $O_{yz(zx)}$ |
| 4 | $H_0$, $H_4$ | $H_{za}$ | $H_2$ | $H_{zb}$ | $H_{x(y)a}$, $H_{x(y)b}$ |
| | $A_1^-$ | $A_2^-$ | $B_1^-$ | $B_2^-$ | $E^-$ |
| 1 | | $J_z$ | | | $J_{x(y)}$ |
| 3 | | $T_{za}$ | $T_{xyz}$ | $T_{zb}$ | $T_{x(y)a}$, $T_{x(y)b}$ |
| 5 | $D_4$ | $D_{za1}$, $D_{za2}$ | $D_2$ | $D_{zb}$ | $D_{x(y)a1}$, $D_{x(y)a2}$, $D_{x(y)b}$ |

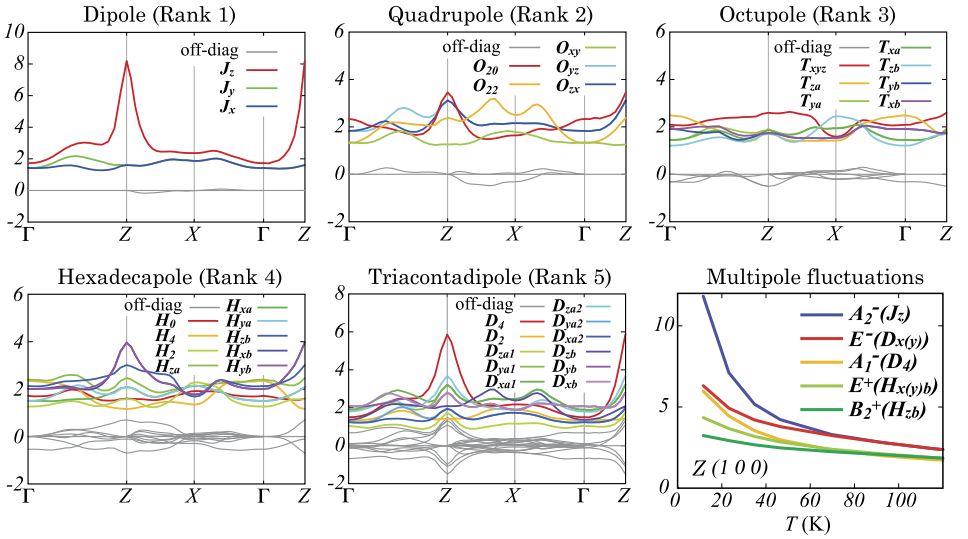


**Fig. 5.** (Color online.) (a–e) Multipole susceptibilities along high-symmetry lines. (f) Temperature dependence of IR-resolved susceptibilities at the $Z$ point.

$$D_x = \begin{pmatrix} & 0.02 & & 0.11 & & 0.65 \\ 0.02 & & -0.08 & & -0.08 & \\ & -0.08 & & 0.11 & & 0.11 \\ 0.11 & & 0.11 & & -0.08 & \\ & -0.08 & & -0.08 & & 0.02 \\ 0.65 & & 0.11 & & 0.02 & \end{pmatrix} \tag{9}$$

where the norms are normalized by $\sum_{\ell m} |A_{\ell m}|^2 = 1$.

### 3.3. Multipole susceptibilities

Now, let us calculate high-rank multipole correlations. The results are summarized in Fig. 5. Here, rank 1 corresponds to the magnetic susceptibilities already discussed, although the magnitude is rescaled by $2/(35g^2)$ due to normalization of norms. Unexpectedly, some high-rank multipole correlations, such as hexadecapole and triacontadipole, are enhanced at the $Z$ point. In our itinerant model, these are some kind of density wave of multipoles, rather than localized multipoles. Interestingly, in this case, these multipole fluctuations have been enhanced by only on-site Hubbard interactions. This is different from the conventional study in the localized systems, where the interactions between high-rank multipoles need to be introduced. Among the enhanced susceptibilities, the most divergent susceptibility implies a possible multipole order. It should be noted that susceptibilities belonging to the same IR can mix with each other, even between different ranks. This effect can be naturally taken into account by diagonalizing the generalized susceptibility $\hat{\chi}^{\mathrm{RPA}}(\mathrm{Q}_0)$. Fig. 5f depicts the temperature dependence of various susceptibilities. The largest $A_2^-$ state, dominated by the dipole $J_z$ component, corresponds to the large-momentum AFM state. Therefore candidates for the HO parameter are first the $E^-$, $A_1^-$ triacontadipole, and second the $E^+$, $B_2^+$ hexadecapole. However, within the RPA this kind of order cannot be realized.

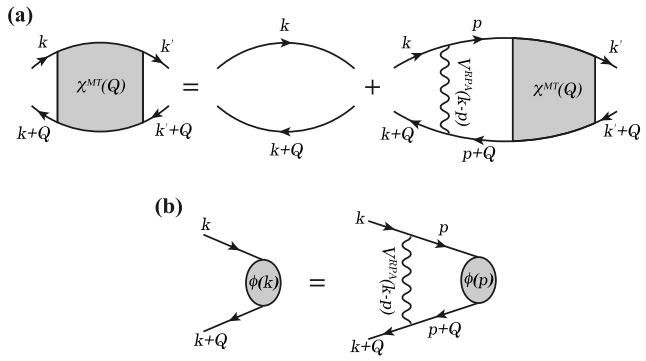


**Fig. 6.** (a) Correlation function for staggered pairing mediated by the RPA susceptibility. (b) The corresponding Bethe–Salpeter equation.

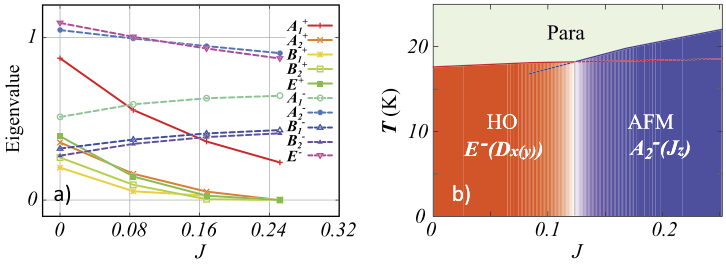


**Fig. 7.** (a) Eigenvalue $\lambda$ of the Bethe–Salpeter equation as a function of $J$. (b) Phase diagram expected from nearly degenerate $E^-$ and $A_2^-$ states, which may account for the experimental $P$–$T$ phase diagram. As the transition temperature increases, we also increase $U$ with $J$.

### 3.4. Beyond RPA

#### 3.4.1. Staggered electron–hole pairing mediated by RPA fluctuations

Generally speaking, the RPA enhances a magnetic channel too much. This is improved by including the mode–mode coupling terms. To study such an effect, we consider here the possibility of a staggered electron–hole pair mediated by the RPA susceptibilities, in analogy with unconventional superconductivity (see Fig. 6). This corresponds to the inclusion of Maki–Thompson (MT) type vertex corrections. The relevant Bethe–Salpeter equation is given by

$$\lambda\phi_{\ell m}(k) = T\sum_{p} V^{\mathrm{RPA}}_{\ell\ell_1,mm_1}(k-p)G^0_{\ell_1\ell'}(p)G^0_{m'm_1}(p+Q_0)\phi_{\ell' m'}(p) \tag{10}$$

where $\phi_{\ell m}(\mathbf{k}) = \langle f^\dagger_{\mathbf{k}\ell} f_{\mathbf{k}+\mathbf{Q}_0 m}\rangle$ is an order parameter for the staggered electron–hole pairs. In the same way, as for the superconducting linearized-gap equation, the eigenvalue $\lambda = 1$ provides the transition temperature. Although the obtained order parameter generally depends on the momentum $\mathbf{k}$, in our calculations order parameters with large $\lambda$ are almost independent of $\mathbf{k}$. Fig. 7a shows the maximum eigenvalue $\lambda$ for each symmetry as a function of $J$, for $U \simeq 2.43$ and $T = 16$ K. In this case rank-5 $E^-$, which has the second largest eigenvalue in the RPA, is relatively enhanced. This rank-5 $E^-$ state and the dipole $A_2^-$ state are nearly degenerate. Eigenvalues of these two states smoothly intersect as a function of $J$. This fact allows one to explain the $P$–$T$ phase diagram. Experimentally, the transition temperature changes smoothly with applying pressure [10,11]. As shown in Fig. 7b, we can easily draw a very similar phase diagram indicating that the rank-5 $E^-$ state is a promising candidate for the HO. Indeed, this rank-5 $E^-$ state is consistent with key features in the HO state, including a breaking of the fourfold rotational symmetry observed in recent experiments [22–25]. On the other hand, in-plane ordered dipole moments, which can be induced in this state, have not yet been observed. It is expected that their magnitude will be very small, as inferred from the fact that the in-plane dipole susceptibility is inactive. The detection of such tiny moments remains an issue for the future.

#### 3.4.2. Higher-order corrections

In the previous section, we have shown that the rank-5 $E^-$ state is a promising candidate for the HO by considering the MT-type vertex corrections. However, in many cases, a higher-order Aslamasov–Larkin (AL) term is important. Let us examine contributions of the AL term and the self-energy corrections (Fig. 8a). We compare here these correction terms in irreducible diagrams. After very complicated calculations [7], we obtain the result in Fig. 8b. It indicates that the conclusion in the previous section is not altered. The magnitude of the AL term is large, but it does not produce a relative difference between the two states, $E^-$ and $A_2^-$. As the AL term can mediate two antiferroic fluctuations, it is crucial to ferroic correlations, but not so important for antiferroic ones.

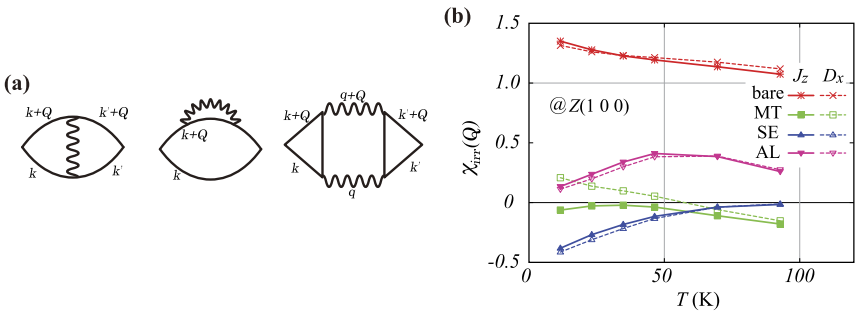


**Fig. 8.** (a) Some vertex corrections, in order: the Maki–Thompson (MT) term, the self-energy correction term, and the Aslamasov–Larkin (AL) term. (b) Each contribution as a function of $T$.

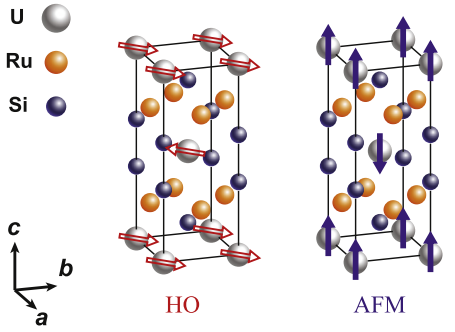


**Fig. 9.** (Color online.) HO and AFM states in terms of the pseudo-spin representation. The HO (AFM) state corresponds to the in-plane ($c$-axis) order of pseudo-spins.

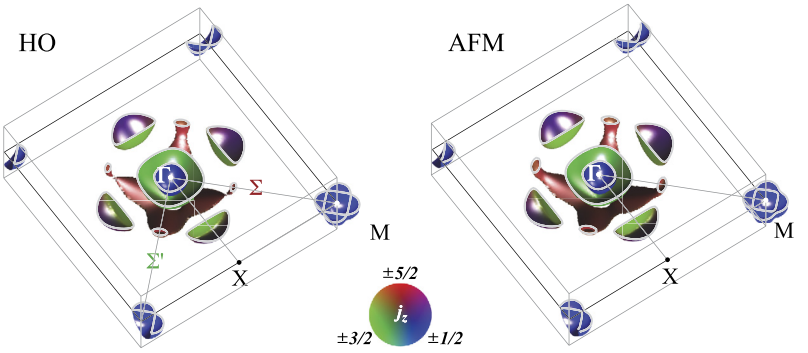


**Fig. 10.** (Color online.) (Left) the Fermi surface in the rank-5 $E^-$ state, and (right) that in the AFM state. The two Fermi surfaces are very similar.

## 4. Ordered states

### *4.1. Rank-5 $E^-$ state and Fermi surface in the ordered states*

In this section, let us consider the physical picture of the rank-5 (triacontadipole) $E^-$ state. The representation matrix of this state is $D_x$ or $D_y$, whilst that of the dipole $A_2^-$ state is $J_z$. These matrices have a large value between $j_z = \pm 5/2$ components. On the other hand, the nested Fermi surface also has a large weight of $\pm 5/2$ components. If we focus on these $j_z$ components, $(D_x, D_y, J_z)$ can be described in the pseudo-spin space of $j_z = \pm 5/2$ by three pseudo-spins $(\sigma_x, \sigma_y, \sigma_z)$. In this case, the in-plane $(\sigma_{x(y)})$ order denotes the HO state, while the $c$-axis $\sigma_z$ order is the AFM state (Fig. 9). The first-order transition from the HO to the AFM state corresponds to the pseudo-spin flop transition.

Which direction the in-plane pseudo-spin turns depends on the in-plane anisotropy. In our calculations, [110] and the corresponding directions are easy axis, but the in-plane anisotropy is not strong. This makes the situation more complicated.

In the ordered states, $\Gamma$ and $Z$ points are identical due to the Brillouin zone folding with $Q_0 = (0\ 0\ 1)$. The outer electron surface around $\Gamma$ and the outer hole surface around $Z$ overlap (Fig. 10). The most parts of carriers in the nested Fermi surfaces vanish with the formation of a small gap $\sim$4 meV below $T_{\mathrm{HO}}$. This can explain the behavior in the Hall measurements [19]. Moreover, the Fermi surface in the HO state is very similar to that in the AFM state, which is consistent

**Table 2**
Comparison of the proposed HO parameters. Multipoles show the main ingredient obtained in our calculations. $\boldsymbol{T}$, **Fourfold**, and $\boldsymbol{M_Q}$ represent time reversal, in-plane fourfold symmetry, and induced dipole moments, respectively. References indicate works proposing order parameters belonging to the listed IRs.

| IRs | Multipoles | $\boldsymbol{T}$ | **Fourfold** | $\boldsymbol{M_Q}$ | References |
|---|---|---|---|---|---|
| $A_1^+$ | $H_4$ | preserved | preserved | none | |
| $A_2^+$ | $H_{za}$ | preserved | preserved | none | [37,39] |
| $B_1^+$ | $O_{22}$ | preserved | preserved | none | |
| $B_2^+$ | $H_{zb}$ | preserved | preserved | none | [31,38] |
| $E^+$ | $(O_{yz}, O_{zx})$ | preserved | lost | none | [27,41–43] |
| $A_1^-$ | $D_4$ | lost | preserved | none | [7] |
| $A_2^-$ | $D_{za1(2)}$ | lost | preserved | large ($\parallel c$) | [36] |
| $B_1^-$ | $T_{xyz}$ | lost | preserved | none | [28,32] |
| $B_2^-$ | $D_{zb}$ | lost | preserved | none | [28,32] |
| $E^-$ | $(D_x, D_y)$ | lost | lost | tiny but finite ($\perp c$) | [7,33,27,44,45] |

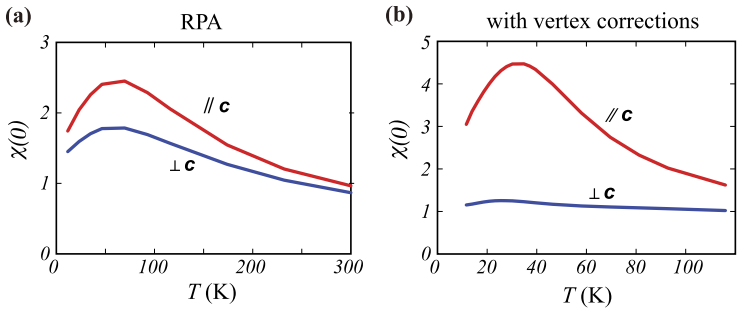


**Fig. 11.** (Color online.) Uniform susceptibilities within the RPA (a), and with the vertex corrections (b). Vertex corrections enhance the magnetic anisotropy.

with the pressure dependence of the quantum oscillation measurements [12,13]. However, the broken fourfold symmetry in the HO state appears as a slight difference between $\Sigma$ and $\Sigma'$ lines. This is compatible with the twofold symmetry observed in recent cyclotron and X-ray diffraction measurements [23–25].

We summarize the proposed theoretical candidates for the HO parameter in Table 2. From this group theoretical classification, we can see what kind of symmetry is preserved or lost in each IR. It will be helpful for future works.

## 5. Itinerant or localized

Finally, let us comment whether the f electrons in $URu_2Si_2$ are itinerant or localized. The uniform susceptibility exhibits a large magnetic anisotropy [4,53]. Generally, a large anisotropy is considered to provide evidence for f electron localization. However, clear CEF splittings have not been observed so far. Rather, several experimental results, such as the resistivity and ARPES measurements [52], implies that the f electrons are itinerant. Thus, it is important to investigate whether the large magnetic anisotropy can be explained on the base of an itinerant model. Fig. 11 illustrates uniform susceptibilities calculated in our model, (a) within the RPA and (b) with the vertex corrections. From the comparison between (a) and (b), we recognize that the effect of vertex corrections, i.e. electron correlations, enhances the magnetic anisotropy. The latter case reproduces well the Ising-like feature observed in experiments [4,53]. It is surprising that such a large anisotropy can be obtained in the framework of an itinerant model. However, a hump structure at around 30 K in the $c$-axis susceptibility calculated with vertex corrections is attributed to the hybridization gap structure of the DOS, not to the Kondo effect. Actually, both this band effect and the Kondo effect should contribute to the temperature dependence of the uniform susceptibilities. This is an interesting future work.

## 6. Summary and perspective

We have reviewed the current status of our understanding of $URu_2Si_2$ based on an itinerant f-electron model. From such a point of view, the promising candidate for the HO parameter is an antiferroic order of a rank-5 (triacontadipole) $E^-$ state. This state is consistent with the recently reported breaking of the fourfold-symmetry, the experimental evidence of which is rapidly increasing. Quite recently, high-resolution X-ray diffraction measurements in ultra clean samples have revealed two-fold orthorhombic lattice distortion in the HO state [24,25]. In such measurements, the sample quality is very important. This may be related to the small anisotropy energy of the in-plane pseudo-spins in the rank-5 $E^-$ state. Further studies are required to clarify the genuine order parameter.

In this study, we have developed a first-principles theoretical approach to clarify several missing link in the heavy-fermion systems, such as, multipole correlations and magnetic anisotropy in the itinerant f-electron systems. These are the

first step to microscopically understand the heavy-fermion systems. To take a step further, we need to consider the effect of electron correlations, for instance, by the DFT+DMFT method [54,55]. It is an interesting future work. Our advanced theoretical approach and its development can provide a powerful tool to unveil many long-standing problems in heavy-fermion materials [56,57].

## Acknowledgements

This review is based on the work in collaboration with T. Shibauchi and Y. Matsuda. We thank K. Ishida, K. Ueda, J. Flouquet, D. Aoki, G. Knebel, F. Bourdarot, M. Sigrist, T.M. Rice, P. Thalmeier, C. Geibel, F. Steglich, Y. Kitaoka, J.A. Mydosh, P.M. Oppeneer, Y. Kuramoto, C.M. Varma, K. Haule, G. Kotliar, P.S. Riseborough, P. Chandra, P. Coleman, R. Caciuffo, J. Schmalian and Y. Zaanen for helpful discussions. This work was partially supported by Grant-in-Aid for the Global COE program "The Next Generation of Physics, Spun from Universality and Emergence", Grant-in-Aid for Scientific Research on Innovative Areas "Heavy Electrons" (20102002, 20102006) from the Ministry of Education, Culture, Sports, Science and Technology (MEXT) of Japan, and KAKENHI (23340095, 24540369) from Japan Society for the Promotion of Science (JSPS).

## References

[1] G. Kotliar, et al., Rev. Mod. Phys. 78 (2006) 865.
[2] K. Held, Adv. Phys. 56 (2007) 829.
[3] M. Imada, T. Miyake, J. Phys. Soc. Jpn. 79 (2010) 112001.
[4] T.T.M. Palstra, et al., Phys. Rev. Lett. 55 (1985) 2727–2730.
[5] M.B. Maple, et al., Phys. Rev. Lett. 56 (1986) 185–188.
[6] J.A. Mydosh, P.M. Oppeneer, Rev. Mod. Phys. 83 (2011) 1301.
[7] H. Ikeda, et al., Nat. Phys. 8 (2012) 528.
[8] Y. Kasahara, et al., Phys. Rev. Lett. 99 (2007) 116402;
Y. Kasahara, et al., New J. Phys. 11 (2009) 055061.
[9] C. Broholm, et al., Phys. Rev. Lett. 58 (1987) 1467.
[10] H. Amitsuka, et al., J. Magn. Magn. Mater. 310 (2007) 214.
[11] E. Hassinger, et al., Phys. Rev. B 77 (2008) 115117.
[12] H. Ohkuni, et al., Philos. Mag. B 79 (1999) 1045.
[13] E. Hassinger, et al., Phys. Rev. Lett. 105 (2010) 216409.
[14] R. Yoshida, et al., Phys. Rev. B 82 (2010) 205108;
R. Yoshida, et al., Sci. Rep. 3 (2013) 2750.
[15] F.L. Boariu, et al., Phys. Rev. Lett. 110 (2013) 156404.
[16] J.-Q. Meng, et al., Phys. Rev. Lett. 111 (2013) 127002.
[17] A.R. Schmidt, et al., Nature 465 (2010) 570–576.
[18] P. Aynajian, et al., Proc. Natl. Acad. Sci. USA 107 (2010) 10383.
[19] K. Behnia, et al., Phys. Rev. Lett. 94 (2005) 156405.
[20] F. Bourdarot, et al., J. Phys. Soc. Jpn. 79 (2010) 064719.
[21] C.R. Wiebe, et al., Nat. Phys. 3 (2007) 96.
[22] R. Okazaki, et al., Science 331 (2011) 439.
[23] S. Tonegawa, et al., Phys. Rev. Lett. 109 (2012) 036401;
S. Tonegawa, et al., Phys. Rev. B 88 (2013) 245131.
[24] S. Tonegawa, et al., Nat. Commun. 5 (2014) 4188.
[25] T. Shibauchi, H. Ikeda, Y. Matsuda, Philos. Mag. (2014), http://dx.doi.org/10.1080/14786435.2014.887861.
[26] S. Kambe, et al., Phys. Rev. Lett. 110 (2013) 246406.
[27] P. Thalmeier, T. Takimoto, Phys. Rev. B 83 (2011) 165110;
P. Thalmeier, T. Takimoto, H. Ikeda, Philos. Mag. (2013), http://dx.doi.org/10.1080/14786435.2013.861615.
[28] P. Santini, G. Amoretti, Phys. Rev. Lett. 73 (1994) 1027;
P. Santini, et al., Phys. Rev. Lett. 97 (2006) 207203.
[29] P. Chandra, et al., Nature 417 (2002) 831–834.
[30] H. Ikeda, Y. Ohashi, Phys. Rev. Lett. 81 (1998) 3723–3726.
[31] F.J. Ohkawa, H. Shimizu, J. Phys. Condens. Matter 11 (1999) L519.
[32] A. Kiss, P. Fazekas, Phys. Rev. B 71 (2005) 054415.
[33] K. Hanzawa, N. Watanabe, J. Phys. Condens. Matter 17 (2005) L419.
[34] C.M. Varma, L. Zhu, Phys. Rev. Lett. 96 (2006) 036405.
[35] S. Elgazzar, et al., Nat. Mater. 8 (2009) 337.
[36] F. Cricchio, et al., Phys. Rev. Lett. 103 (2009) 107202.
[37] K. Haule, G. Kotliar, Nat. Phys. 5 (2009) 796–799.
[38] H. Harima, K. Miyake, J. Flouquet, J. Phys. Soc. Jpn. 79 (2010) 033705.
[39] H. Kusunose, H. Harima, J. Phys. Soc. Jpn. 80 (2011) 084702.
[40] Y. Dubi, A.V. Balatsky, Phys. Rev. Lett. 106 (2011) 086401.
[41] S. Fujimoto, Phys. Rev. Lett. 106 (2011) 196407.
[42] C. Pépin, et al., Phys. Rev. Lett. 106 (2011) 106601.
[43] P.S. Riseborough, B. Coqblin, S.G. Magalhaes, Phys. Rev. B 85 (2012) 165116.
[44] J.G. Rau, H.-Y. Kee, Phys. Rev. B 85 (2012) 245112.
[45] P. Chandra, P. Coleman, R. Flint, Nature 493 (2013) 621–626.
[46] P.M. Oppeneer, et al., Phys. Rev. B 82 (2010) 205103.
[47] J. Kuneš, et al., Comput. Phys. Commun. 181 (2010) 1888, http://www.wien2k.at/reg_user/unsupported/wien2wannier.
[48] K. Kuroki, et al., Phys. Rev. Lett. 101 (2008) 087004.

[49] P. Blaha, et al., WIEN2K, An Augmented Plane Wave + Local Orbitals Program for Calculating Crystal Properties, Karlheinz Schwarz, Techn. Universität, Wien, Austria, 2001.
[50] G. Cordier, et al., J. Less-Common Met. 110 (1985) 327.
[51] N. Marzari, D. Vanderbilt, Phys. Rev. B 56 (1997) 12847;
I. Souza, N. Marzari, D. Vanderbilt, Phys. Rev. B 65 (2001) 035109;
A.A. Mostofi, et al., Comput. Phys. Commun. 178 (2008) 685, http://www.wannier.org/.
[52] I. Kawasaki, et al., Phys. Rev. B 83 (2011) 235121.
[53] A.P. Ramirez, et al., Phys. Rev. Lett. 68 (1992) 2680–2683.
[54] Z.P. Yin, K. Haule, G. Kotliar, arXiv:1311.1188.
[55] A.B. Shick, et al., Phys. Rev. B 89 (2014) 041109(R).
[56] H. Ikeda, M.-T. Suzuki, R. Arita, preprint.
[57] T. Nomoto, H. Ikeda, preprint.